Available online at www.sciencedirect.com
SCIENCE DIRECT®
Journal of Nuclear Materials 323 (2003) 72–80
journal of nuclear materials
www.elsevier.com/locate/jnucmat

Influence of Nb concentration in the α-matrix on the corrosion behavior of Zr–*x*Nb binary alloys

Yong Hwan Jeong *, Hyun Gil Kim, Dae Jung Kim, Byung Kwon Choi, Jun Hwan Kim

Zirconium Fuel Cladding Team, Korea Atomic Energy Research Institute, P.O. Box 105, Yuseong, Daejeon 305-600, South Korea

Received 8 August 2002; accepted 14 August 2003

Abstract

The influence of the Nb concentration in the α-matrix on the corrosion behavior of Zr–*x*Nb ($x = 0$–0.6 wt%) binary alloys was evaluated using a static autoclave in the temperature range from 300 to 500 °C. Corrosion tests and precipitate analysis of Zr–*x*Nb binary alloys showed that corrosion resistance increased with the increase of the Nb concentration in the α-matrix, and the best corrosion resistance was obtained when the Nb concentration was nearly at its equilibrium solubility limit at all test temperatures. The alloys containing a higher Nb concentration than their equilibrium solubility also showed good corrosion resistance, which could be attributed mainly to the formation of Nb-precipitates, resulting in an equilibrium Nb concentration in the α-matrix. These results imply that the corrosion resistance of Nb-containing Zr-alloys can be controlled by the Nb concentration in the α-matrix rather than the Nb-precipitates.

PACS: 81.65.M; 81.65.K; 42.81.B

1. Introduction

Corrosion properties of Zr-alloys for nuclear fuel cladding materials in high temperature aqueous solutions are mainly affected by the material parameters which include alloying elements, precipitates, and microchemistry. The effect of metallurgical parameters on the corrosion behavior of Zr-based alloys has been studied extensively [1–3]. Recently, advanced Zr-based alloys have been required for severe operating conditions such as an increased burn-up and a higher operation temperature.

Several advanced Zr-alloys such as Zirlo (Zr–1.0Nb–1.0Sn–0.1Fe) [1], M5(Zr–1Nb–O) [2] and NDA (Zr–0.1Nb–1.0Sn–0.27Fe–0.16Cr) [3] have been developed and are being tested in reactors as substitutes for commercial Zircaloy-4. The fact that Nb was selected as a major alloying element in the Zr-based alloy has become a common characteristic for the newly developed fuel claddings [1–5]. Nb has not been considered as an alloying element in conventional Zircaloy-4 which has been used in pressurized water reactors. As the corrosion properties of the Nb-containing Zr-alloys are known to highly rely on the microstructure, it is essentially required to investigate the effect of the Nb-content and the metallurgical parameters on the corrosion of Zr–*x*Nb binary alloys for a better understanding of the mechanism of corrosion resistance.

From the studies on the effect of the β phase on corrosion, it has been reported that the corrosion rate of Zr–Nb alloy increased with the formation of the β_{Zr} phase (~20 wt% Nb) but decreased with the formation of the β_{Nb} phase (~80 wt% Nb) [6,7]. When Zr–Nb alloys were annealed in the $\alpha + \beta_{Nb}$ temperature range below the monotectoid temperature (610 °C) after beta

* Corresponding author. Tel.: +82-42 868 2322; fax: +82-42 862 0432.
E-mail address: yhjeong@kaeri.re.kr (Y.H. Jeong).

0022-3115/$ - see front matter © 2003 Elsevier B.V. All rights reserved.
doi:10.1016/j.jnucmat.2003.08.031

quenching, the β_{Nb} phase can be produced by the phase transformation of $\alpha' \rightarrow \alpha + \beta_{Zr} \rightarrow \alpha + \beta_{Nb}$. [9–13]. Also, Urbanic [7,8] reported that the corrosion resistance was enhanced with the precipitation of the β_{Nb} phase in a Zr–2.5Nb pressure tube under irradiation conditions.

In our previous study [14,15] on the effect of the second phase and the Nb solubility on the corrosion of the Zr–*x*Nb alloys, it has been suggested that the corrosion resistance of the alloys containing the β_{Nb} phase was not improved by β_{Nb} itself but by the equilibrium Nb concentration in the matrix resulting from the reduction of the Nb concentration in the matrix by the formation of the β_{Nb} phase.

Thus, there is still uncertainty on the mechanism of corrosion resistance of the Nb-containing Zr-alloys. The present study was carried out to identify which factor, i.e. the equilibrium Nb concentration in the α-matrix or the precipitates, plays the dominant role in the corrosion resistance of Nb-containing Zr-alloys.

2. Experimental procedure

Eight Zr–*x*Nb binary alloys ($x = 0$, 0.05, 0.1, 0.2, 0.3, 0.4, 0.5 and 0.6 in wt%) were prepared by the vacuum arc remelting (VAR) method. Sponge Zr and high purity Nb were used as raw materials to simulate the commercial alloys. The chemical compositions of Zr–*x*Nb alloys are given in Table 1. Minor elements like Fe and Cr which were introduced from the sponge zirconium were also observed in all samples. The ingots were annealed, hot-rolled and cold-rolled, and finally annealed at 590 °C for 3 h. The microstructures of the samples were also investigated using transmission electron microscope (TEM)/energy dispersive spectroscope (EDS).

Corrosion tests were performed in water at 300 and 360 °C and in steam at 400, 450, and 500 °C using static autoclaves according to the ASTM G2 method. The corrosion rates were evaluated by the discontinuous gravimetric method. The characteristics of the oxide layer on the corroded samples which were prepared to have an equal weight gain by the control of exposure time were examined by scanning electron microscope (SEM), X-ray diffraction (XRD), and TEM. Particularly, the synchrotron X-ray (Line 3C2) at the Pohang Accelerator Laboratory in Korea was used to analyze the oxide characteristics. It was reported in our previous study [14] that the Synchrotron X-ray scattering is a more accurate technique to detect the crystallography of a thin oxide film than the conventional low angle XRD. For the synchrotron X-ray analysis, the θ–2θ method was also used. The fraction of tetragonal-ZrO_2 (Xt) was calculated using the following equation [16]:

$$\mathrm{Xt} = (1\,1\,1)\mathrm{t}/[(1\,1\,1)\mathrm{t} + (-1\,1\,1)\mathrm{m} + (1\,1\,1)\mathrm{m}], \quad (1)$$

where (1 1 1)t, (−1 1 1)m and (1 1 1)m are the integrated intensities of the (1 1 1) reflection of tetragonal-ZrO_2, the (−1 1 1) reflection of monoclinic-ZrO_2, and the (1 1 1) reflection of monoclinic-ZrO_2, respectively.

3. Results and discussion

3.1. Corrosion behavior of Zr–xNb alloys at different temperatures

Fig. 1 shows the corrosion behavior of Zr–*x*Nb binary alloys in water at 300 and 360 °C. It was observed that the corrosion resistance was dependent on the Nb content. At 300 °C (Fig. 1(a)), the unalloyed Zr exhibited an accelerated corrosion, showing the spalling phenomena of oxide scales after 2500 h. The corrosion resistance increased with the addition of Nb, and the lowest weight gain was observed in the Zr–0.1wt% Nb alloy. However, in the range of Nb content above 0.2 wt%, the corrosion resistance continuously decreased with the increase of the Nb content. The corrosion behavior at 360 °C (Fig. 1(b)) was similar to that at 300 °C. At 360 °C, the lowest weight gain was observed in the Zr–0.2wt%Nb alloy while the Zr–0.1wt%Nb alloy which had shown the lowest weight gain at 300 °C exhibited a high corrosion rate showing the oxide spalling phenomena.

Fig. 2 shows the corrosion behavior of Zr–*x*Nb binary alloys in steam at 400, 450 and 500 °C. The lowest

Table 1
Chemical compositions of Zr–*x*Nb binary alloys

Nominal composition (wt%)	Nb	0.00	0.05	0.10	0.20	0.30	0.40	0.50	0.60
Analyzed composition	Nb (wt%)	0.00	0.05	0.11	0.21	0.33	0.42	0.51	0.62
	Fe (ppm)	720	680	720	720	690	700	710	660
	Cr (ppm)	83	75	85	90	83	78	81	94
	O (ppm)	677	660	705	673	672	687	704	710
	C (ppm)	33	37	36	35	38	36	35	36
	Zr					Balance			

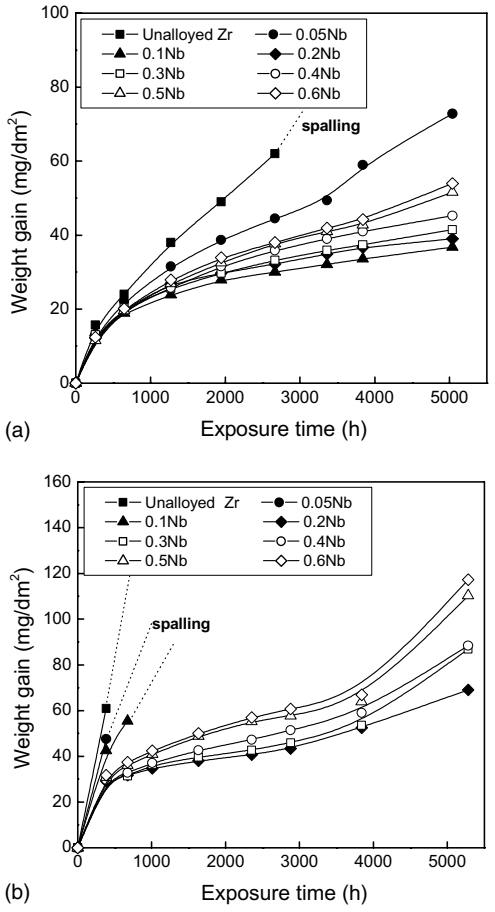

Fig. 1. Corrosion behavior of Zr–xNb binary alloys in water at 300 (a) and 360 °C (b).

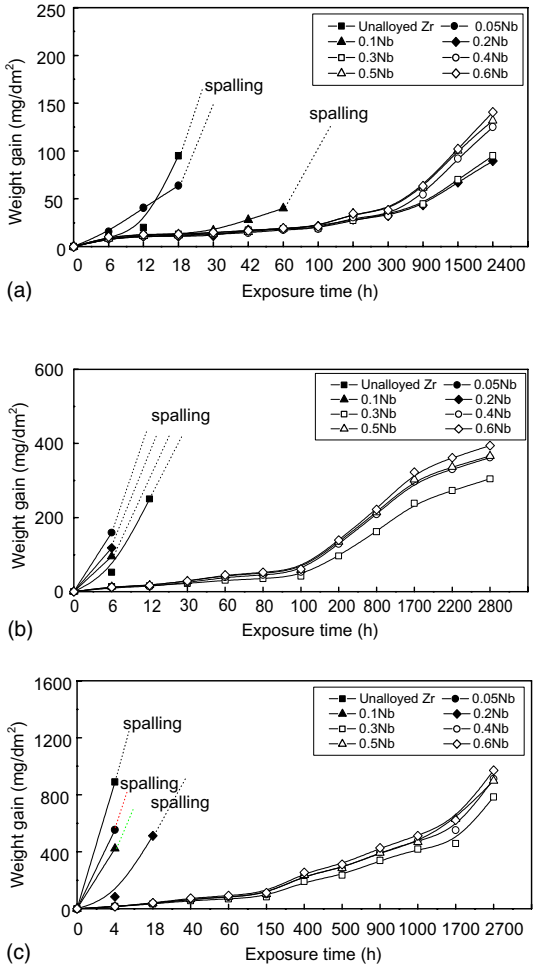

Fig. 2. Corrosion behavior of Zr–xNb binary alloys in steam at 400 (a), 450 (b) and 500 °C (c).

corrosion rate at 400 °C was observed in the Zr–0.2Nb and Zr–0.3Nb alloys. At 450 and 500 °C, the Zr–0.3Nb alloy showed the best corrosion resistance while Zr–0.2Nb which had shown a good corrosion resistance at 400 °C exhibited a bad corrosion resistance showing the oxide spalling. The corrosion behaviors of Zr–xNb alloys are divided into two groups, i.e. good corrosion resistance of Zr–Nb alloys containing a low Nb content and bad corrosion resistance of Zr–Nb alloys containing a high Nb content. There was a critical Nb content in Zr–xNb alloys between the good corrosion resistant alloys and the bad corrosion resistant alloys.

Fig. 3 shows the relationship between the final weight gain and Nb content in the Zr–Nb binary alloy after a corrosion test at different temperatures. The weight gains were rapidly decreased to a certain Nb content where the weight gain was a minimum level, and then slightly increased with the increase of the Nb content. This critical Nb content showing the best corrosion resistance was changed from 0.1 to 0.3 wt% with the increase of test temperature from 300 to 500 °C. This

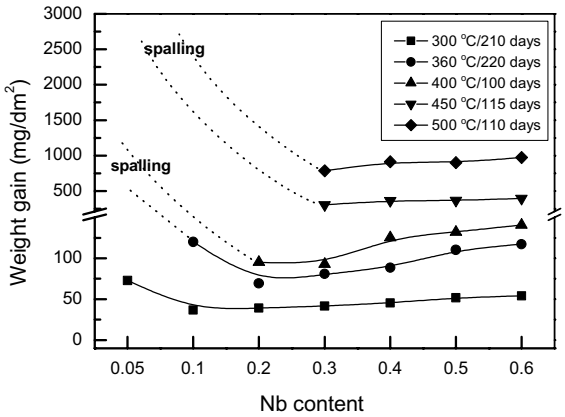

Fig. 3. Correlation between the final weight gain and Nb content in Zr–xNb binary alloys.

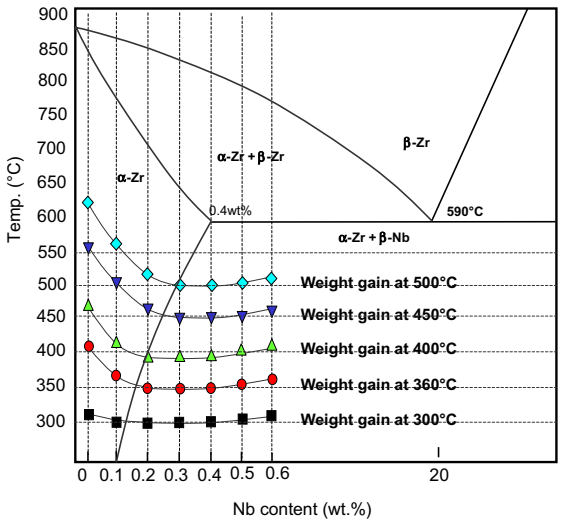

Fig. 4. Zr–Nb binary phase diagram showing the correlation between the corrosion resistance and Nb content at various temperatures.

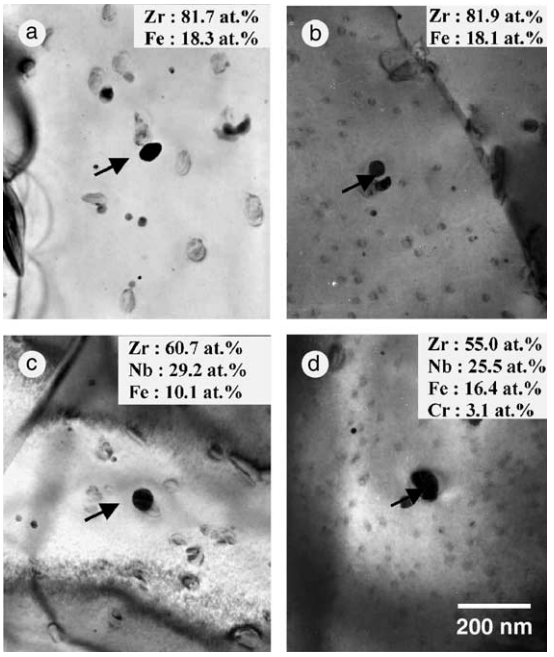

Fig. 5. TEM images and EDS data on the precipitates in Zr–0.2Nb (a), Zr–0.3Nb (b), Zr–0.4Nb (c) and Zr–0.5Nb alloy (d) before corrosion test.

implies that the corrosion behaviors of Zr–xNb alloys are different depending on the test temperature. An increased test temperature makes the solubility of the Nb in the α-matrix shift upward, resulting in the increase of the equilibrium Nb concentration in the α-matrix and a change of the second phase.

In order to investigate the correlation between the corrosion resistance and the equilibrium Nb concentration in the Zr–Nb binary alloys more clearly, the weight gains after a corrosion test were superimposed onto the phase diagram of the Zr–Nb binary alloy, which are shown in Fig. 4. It is clearly shown that the alloys containing Nb less than their solubility showed the worst corrosion resistance at all the tested temperatures. It is thus deduced that the main metallurgical factor controlling the corrosion behavior of Zr–xNb binary alloys could be the Nb concentration in the matrix.

3.2. Microstructure

Fig. 5 shows the results of the TEM/EDS studies on the Zr–xNb binary alloys before corrosion testing. All the alloys were composed of fully recrystallized structures due to the final annealing at a high temperature of 590 °C, and showed a similar morphology and distribution of the precipitates. However, there was a little difference in chemical composition and crystal structure of precipitates in the Zr–xNb alloys as shown in the EDS data. In Zr–0.2Nb and Zr–0.3Nb alloy (Fig. 5(a) and (b)), the Zr_3Fe type precipitates (orthorhombic, $a = 0.3320$ nm, $b = 1.098$ nm, $c = 0.8800$ nm) were observed even though Fe was not intentionally added in the sample. The formation of Zr_3Fe type precipitate resulted from the Fe in the sponge zirconium. The maximum solubilities of Fe and Cr in Zr–1.4Sn alloy are known to be about 120 ppm at 820 °C and 200 ppm at 860 °C, respectively [17]. The Fe content in the sponge zirconium used in this study was about 700 ppm. Thus, most Fe in sponge Zr would be precipitated as Fe-containing precipitates. In Zr–0.4Nb (Fig. 5(c)) and Zr–0.5Nb alloys (Fig. 5(d)), Zr $(Nb,Fe,Cr)_2$ type precipitates (hcp, $a = 0.5401$ nm $c = 0.8665$ nm) were observed. This precipitate was identified to be the Zr $(NbFe)_2$ type with a hexagonal structure by selected area diffraction (SAD) analysis. The $(ZrNb)_3Fe$ type precipitates with a orthorhombic structure were not found in these alloys.

To analyze the supersaturated or soluble Nb concentration in the matrix, EDS analysis was performed for all the specimens. But it was not successful in analyzing the exact Nb concentration in the matrix owing to the limited resolution of the EDS. However, it can be expected that in the samples having a Nb content less than 0.3 wt%, Nb would be soluble in the matrix without supersaturation or precipitation. It is considered that the difference in crystal structure and chemical composition of the precipitates mainly results from the correlation between the addition of Nb and the Nb solubility in the Zr–xNb binary alloys.

Fig. 6 shows the results of the TEM/EDS studies on the Zr–xNb binary alloys after corrosion testing in steam

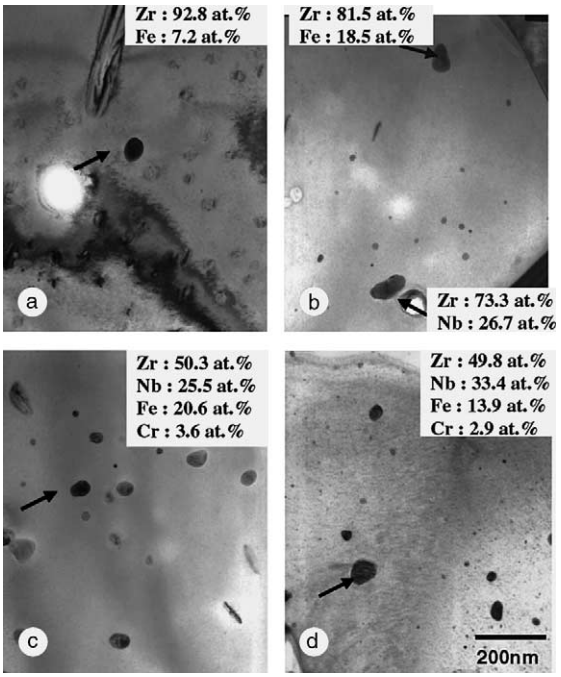

Fig. 6. TEM images and EDS spectra on the precipitates of Zr–0.2Nb (a), Zr–0.3Nb (b), Zr–0.4Nb (c) and Zr–0.5Nb alloy (d) after corrosion test at 400 °C for 1000 h.

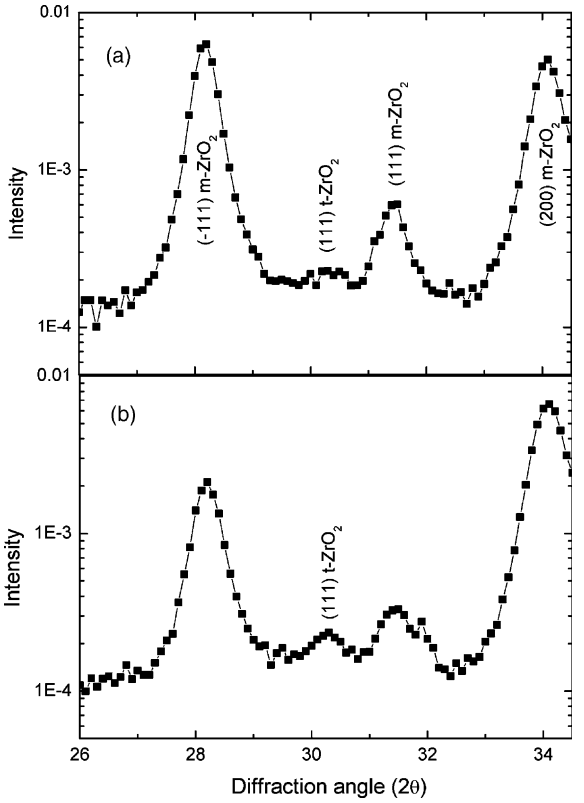

Fig. 7. Synchrotron XRD patterns on the oxides formed in Zr–0.05Nb (a) and Zr–0.5Nb alloy (b) after corrosion test at 400 °C.

at 400 °C for 1000 h. No remarkable difference in the chemical composition of the precipitates in the Zr–xNb alloys after corrosion testing was observed. However, in the case of the Zr–0.3Nb alloy, Nb-containing precipitates besides Fe-containing precipitates were also observed. It could have resulted from the difference of Nb solubility with temperature. Nb-containing precipitates were not observed in the sample annealed at 590 °C before the corrosion test since the Nb solubility was higher than 0.3 wt% at this temperature, while they were observed in the sample tested at 400 °C since the Nb solubility was lower than 0.3 wt% at 400 °C. This means that some of the supersaturated Nb in the matrix is precipitated as Nb-containing precipitates during the corrosion testing, thus maintaining the equilibrium Nb concentration in the α-matrix. Therefore it is possible to suggest that the alloys containing Nb more than their solubility showed good corrosion resistance due to the equilibrium Nb concentration in the matrix.

3.3. Oxide characteristics

Fig. 7 shows the Synchrotron XRD patterns on the oxides formed in Zr–0.05Nb and Zr–0.5Nb alloys having an equal weight gain of 30 mg/dm^2 after the corrosion test in steam at 400 °C. The intensity of (1 1 1) tetragonal ZrO_2 in Zr–0.05Nb alloy having a Nb less than its solubility looks similar to that in the Zr–0.5Nb alloy having Nb more than its solubility. Therefore, to clearly investigate the ratio of tetragonal ZrO_2/monoclinic ZrO_2, the fractions of tetragonal ZrO_2 in both samples were calculated using Eq. (1).

Fig. 8 shows the fractions of tetragonal ZrO_2 in the oxide formed in Zr–0.05Nb and Zr–0.5Nb alloys after

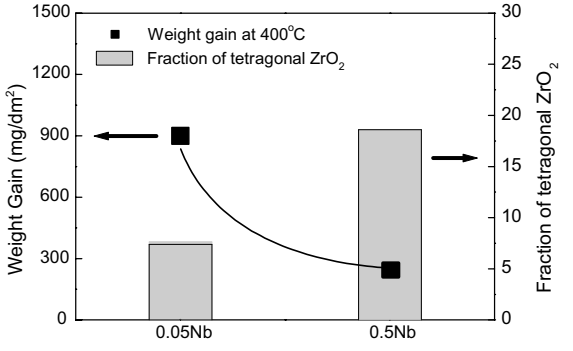

Fig. 8. Fraction of tetragonal ZrO_2 in the oxide formed in Zr–0.05Nb and Zr–0.5Nb alloy (equal weight gain of 30 mg/dm^2).

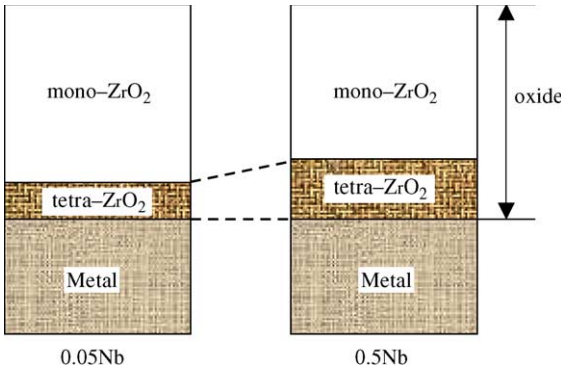

Fig. 9. Illustration for the variation of the oxide structure with Nb content.

the corrosion test at 400 °C. The weight gains were also superimposed onto this graph to show the correlation between the fractions of tetragonal ZrO_2 and the weight gain. The fraction of tetragonal ZrO_2 in the Zr–0.5Nb alloy which showed a low weight gain is much higher than that in the Zr–0.05Nb alloy which showed a high weight gain. The tetragonal ZrO_2 is well known to have a protective property against the oxidation of Zr alloys, and many researchers have reported that the alloy having a good corrosion resistance showed a high fraction of tetragonal ZrO_2 in the oxide [18–21].

Fig. 9 shows the schematic diagram illustrating the variation of oxide structure with Nb content. Even though both samples had an equal oxide thickness, the fraction of tetragonal ZrO_2 in the oxide formed on the Zr–0.5Nb alloy was higher than that in the Zr–0.05Nb alloy. The present results corresponded well to the reported one which showed a high fraction of tetragonal ZrO_2 in the high corrosion resistant alloys [18–21].

Fig. 10 shows the SEM images in a plane view of the oxide at the metal-oxide interfaces formed in Zr–0.05Nb, Zr–0.3Nb and Zr–0.5Nb alloys having an equal weight gain of 30 mg/dm^2 after the corrosion test in steam at 400 °C. The SEM specimens were prepared by dissolving metal parts in the corroded sample. The oxide morphology of Zr–0.05Nb alloy showed a protruded shape which could have resulted from the grain boundary of the matrix.

The Zr–0.3Nb alloy exhibited a uniform oxide surface (Fig. 10(b)) and the Zr–0.5Nb alloy showed a somewhat non-uniform oxide at the metal-oxide interface (Fig. 10(c)). A difference in the morphology of the developing oxide at the metal-oxide interface could be closely related to the corrosion resistance of the tested alloys. Usually, the excellent corrosion resistant alloy showed an uniform oxide interface. Thus it can be considered that a different oxide morphology is attributed to a different Nb concentration. A lower Nb concentration than its solubility results in a protruded shape like Fig. 10(a), while a higher value gives a smooth shape as Fig. 10(b). A somewhat non-uniform oxide layer could be related to the Nb- and Fe-containing precipitates. It is thought that the Nb concentration in the matrix plays an important role in the characteristics of oxide growth in the Zr–Nb alloys.

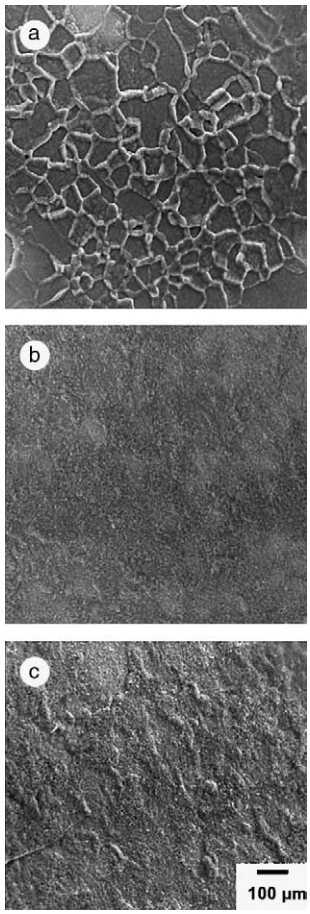

Fig. 10. SEM images on the oxide surfaces at the metal-oxide interfaces formed in Zr–0.05Nb (a), Zr–0.3Nb (b) and Zr–0.5Nb alloy (c) after corrosion test at 400 °C (equal weight gain of 30 mg/dm^2).

Fig. 11 shows the cross-sectional TEM images of the oxide formed on Zr–0.05Nb, Zr–0.3Nb and Zr–0.5Nb alloys having an equal weight gain of 30 mg/dm^2 after the corrosion test in steam at 400 °C. The oxide formed in the Zr–0.05Nb alloy was mainly composed of equiaxed oxide grains (Fig. 11(a)). The Zr–0.2Nb alloy showing an excellent corrosion resistance was mainly composed of columnar oxide grains (Fig. 11(b)). Meanwhile, the oxide formed in the Zr–0.5Nb alloy exhibited a mixture of equiaxed and columnar oxide grains (Fig. 11(c)). Regarding the oxygen diffusion in the

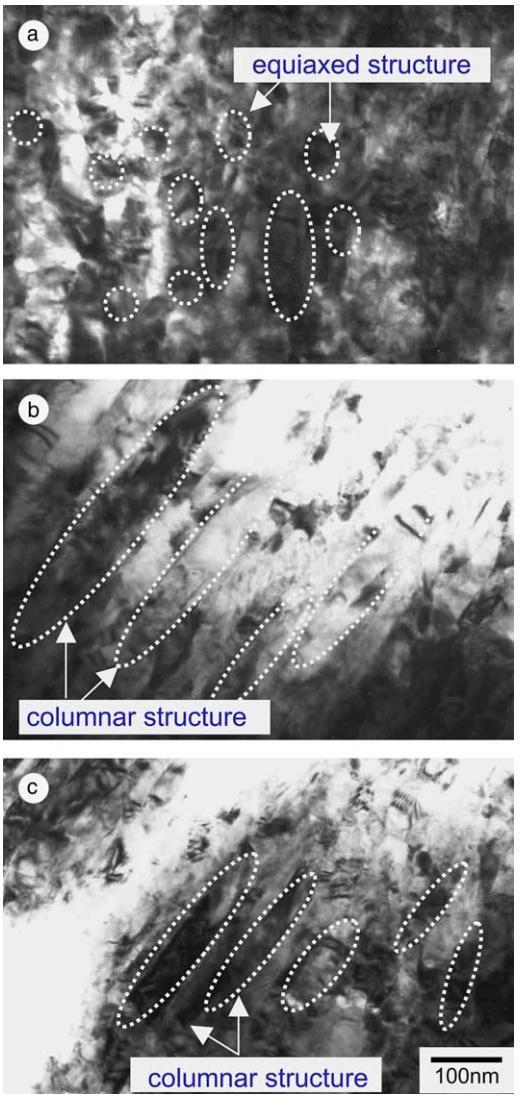

Fig. 11. Cross-sectional TEM images on the oxide-metal interfaces formed in Zr–0.05Nb (a), Zr–0.3Nb (b) and Zr–0.5Nb (c) alloys after corrosion test at 400 °C (equal weight gain of 30 mg/dm^2).

oxide, Godlewski has reported that oxygen transport occurred principally by grain boundary diffusion and the boundary diffusion coefficient was 10^8 times higher than that for a bulk diffusion [22]. Also, it is reported that the equiaxed oxide structure usually has a high fraction of grain boundary which could be an open structure and sometimes contains microcracks, while the columnar structure is more protective than the equiaxed structure against oxygen diffusion [23–25]. Therefore, the present results correspond well to the previous results in terms of the correlation between the oxide structure and corrosion resistance.

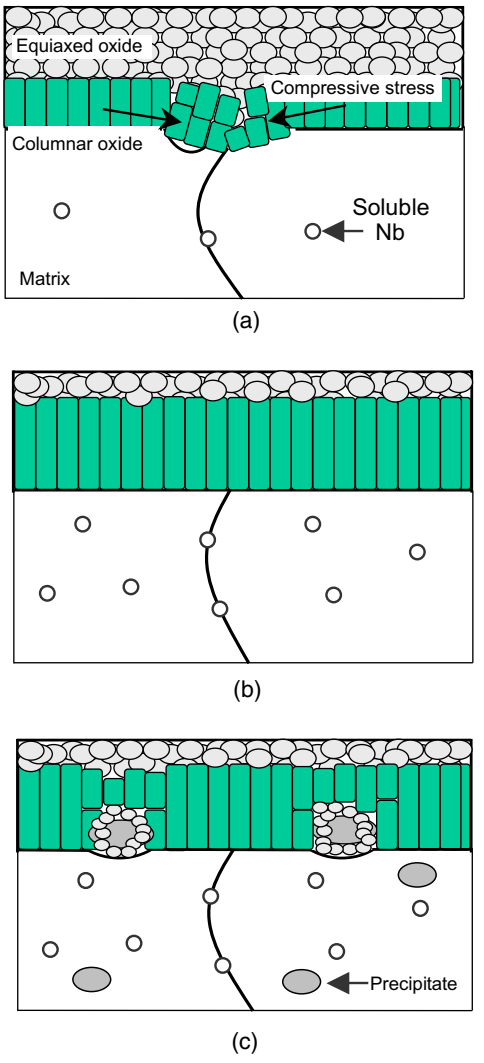

Fig. 12. Schematic diagrams illustrating the correlation between the corrosion behavior and the Nb concentration in the matrix; (a) Nb < equilibrium concentration, (b) Nb = equilibrium concentration and (c) Nb > equilibrium concentration.

3.4. Correlation between the corrosion resistance and the Nb concentration in the α-matrix

Fig. 12 shows the schematic diagrams illustrating the correlation between the corrosion behavior and the Nb concentration in the α-matrix. Based on the corrosion behavior, oxide characteristics, and precipitates observation, the correlation between the corrosion resistance and the Nb content in Zr–*x*Nb alloys could be explained from the viewpoint of the Nb concentration in the matrix and the oxide properties. The corrosion behavior could be divided into three categories depending on the Nb concentration in the matrix; (1) in case of the Nb concentration less than its solubility (Nb $\leqslant$ 0.2 wt%),

(2) equal to its solubility (Nb = 0.3 wt%), and (3) more than its solubility (Nb $\geqslant$ 0.5 wt%).

If the Nb concentration in the matrix is less than its solubility, the corrosion is preferentially accelerated in the grain boundary of the matrix due to the high energy level resulting from microstructural defaults (Fig. 12(a)). When the Nb concentration in the matrix is nearly at its solubility, it helps to prevent the preferential growth in the grain boundary and forms the columnar oxides which are known as a protective oxide structure against oxidation. In case that the Nb concentration in the matrix is more than its solubility, Nb-precipitates which also participate in the corrosion reaction are observed in the matrix.

This indicates that the additional effect of Nb-precipitates besides the matrix would be expected on the corrosion. During the corrosion test, the precipitates usually remain in the oxide layer in the initial stage and then they are finally oxidized, resulting in the change of the oxide structure near the precipitates from columnar grains to equiaxed ones. Thus, alloy containing Nb-precipitates showed a slightly higher corrosion rate than the alloy having an equilibrium Nb concentration without Nb-precipitates. From these results, it could be concluded that the Nb concentration in the matrix plays a dominant role in the control of corrosion rate, and the excellent corrosion resistance is always obtained only when the Nb concentration in the matrix is nearly at its solubility.

4. Conclusions

In this study, the corrosion tests and oxide characterization for the Zr–xNb (x = 0–0.6 wt%) binary alloys were performed in order to evaluate the effect of the Nb content and the Nb concentration in the α-matrix on the corrosion of the Nb-containing Zr-alloys. The results of the corrosion tests at different temperatures of 300–500 °C indicated that the best corrosion resistance was always obtained only when the Nb concentration in the α-matrix was nearly at its equilibrium solubility. Detailed observation on the oxide by using the Synchrotron XRD, SEM and TEM/EDS supported the corrosion results. The critical Nb concentration showing the best corrosion resistance increased with the increase of test temperature owing to the change of equilibrium Nb solubility.

Alloys containing a higher Nb concentration than its equilibrium solubility also revealed a good corrosion resistance due to the additional effect of Nb-precipitate as well as the equilibrium Nb concentration in the α-matrix. It is concluded from the present study that the corrosion resistance of Nb-containing Zr-alloys can be controlled by the Nb concentration in the α-matrix rather than Nb-precipitates.

Acknowledgements

The authors would like to express their appreciation to the Ministry of Science and Technology (MOST) of the Republic of Korea for the support of this work through the mid- and long-term nuclear R&D project.

References

[1] G.P. Sabol, G.R. Kilp, M.G. Balfour, E. Roberts, Zirconium in the Nuclear Industry, ASTM STP, vol. 1023, 1989, p. 227.
[2] J.P. Mardon, G. Garner, P. Beslu, D. Charquer, J. Senevat, Proceedings of the 1997 International Topical Meeting on LWR Fuel Performance, Portland, OR, 2–6 March 1997, p. 405.
[3] K. Yamate, A. Oe, M. Hayashi, T. Okamoto, H. Anada, S. Hagi, Proceedings of the 1997 International Topical Meeting on LWR Fuel Performance, Portland, OR, 2–6 March 1997, p. 318.
[4] A.V. Nikulina, Y.K. Bibilashvili, P.P. Markelov, M.M. Peregu, V.A. Koterekhov, A.F. Lositsky, N.Y. Kuzmenko, Y.P. Shevnin, V.K. Shamardin, G.P. Kobylyansky, A.E. Novoselov, Zirconium in the Nuclear Industry, ASTM STP, vol. 1295, 1996, p. 785.
[5] S. Suzuki, K. Murakami, T. Takahashi, Proceedings of the 1994 International Topical Meeting on LWR Fuel Performance, West Palm Beach, Florida, 17–21 April 1994, p. 352.
[6] G.P. Sabol, R.J. Comstock, U.P. Nayak, Zirconium in the Nuclear Industry, ASTM STP, vol. 1354, 2000, p. 525.
[7] V.F. Urbanic, R.W. Gilbert, IAEA Technical Committee Meeting on Fundamental Aspects of Corrosion of Zr-based Alloys for Water Reactor Environments, Portland, Oregon, 11–15 September 1989, p. 262.
[8] V.F. Urbanic, M. Griffith, Zirconium in the Nuclear Industry, ASTM STP, vol. 1354, 2000, p. 641.
[9] V.N. Shishov, A.V. Nikulina, V.A. Markelov, Zirconium in the Nuclear Industry, ASTM STP, vol. 1295, 1996, p. 603.
[10] S.A. Averin, V.L. Panchenko, A.V. Kozlov, Zirconium in the Nuclear Industry, ASTM STP, vol. 1354, 2000, p. 105.
[11] S. Banerjee, S.J. Vijayakar, R. Krishnan, J. Nucl. Mater. 62 (1976) 229.
[12] S.A. Aldridge, B.A. Chedle, J. Nucl. Mater. 42 (1972) 32.
[13] M.T. Javanovic, Y. Ma, R.L. Eadie, J. Nucl. Mater. 244 (1997) 141.
[14] Y.H. Jeong, K.O. Lee, H.G. Kim, J. Nucl. Mater. 302 (2002) 9.
[15] Y.H. Jeong, H.G. Kim, T.H. Kim, J. Nucl. Mater. 317 (2003) 1.
[16] R.C. Garvie, P.S. Nicholson, J. Am. Ceram. Soc. 55 (1972) 303.
[17] D. Charquet, R. Hahn, E. Ortlieb, J.P. Gros, Zirconium in the Nuclear Industry, ASTM STP, vol. 1023, 1988, p. 405.
[18] J. Godlewski, Zirconium in the Nuclear Industry, ASTM STP, vol. 1245, 1994, p. 663.
[19] H. Anada, K. Takeda, Zirconium in the Nuclear Industry, ASTM STP, vol. 1295, 1996, p. 35.

[20] K. Takeda, H. Anada, Zirconium in the Nuclear Industry, ASTM STP, vol. 1354, 2000, p. 592.
[21] F. Gazarolli, H. Seidel, R. Tricot, J.P. Gros, Zirconium in the Nuclear Industry, ASTM STP, vol. 1132, 1991, p. 395.
[22] J. Godlewski, J.P. Gros, M. Lambertin, J.F. Wadier, H. Weidinger, Zirconium in the Nuclear Industry, ASTM STP, vol. 1132, 1991, p. 416.
[23] D. Pecher, J. Godlewski, P. Billot, J. Thomazet, Zirconium in the Nuclear Industry, ASTM STP, vol. 1295, 1996, p. 94.
[24] B. Wadman, Z. Lai, H.O. Andren, A.-L. Nystrom, P. Rudling, H. Pettersson, Zirconium in the Nuclear Industry, ASTM STP, vol. 1245, 1994, p. 579.
[25] H. Anada, B.J. Herb, K. Nomoto, S. Hagi, R.A. Graham, T. Kuroda, Zirconium in the Nuclear Industry, ASTM STP, vol. 1295, 1996, p. 74.